Longitudinal variability of geomorphic response to floods

Joel S. Sholtes,[1]* **Steven E. Yochum,**[2] **Julian A. Scott**[2] **and Brian P. Bledsoe**[3]
[1] Sedimentation and River Hydraulics Group, Bureau of Reclamation
[2] National Stream and Aquatic Ecology Center, US Forest Service
[3] College of Engineering, University of Georgia

*Correspondence to: Joel S. Sholtes, Bureau of Reclamation, Denver Federal Center, PO BOX 250007, MC 86-68240, Denver, CO 80225. E-mail: jsholtes@gmail.com

ESPL

Earth Surface Processes and Landforms

ABSTRACT: Morphodynamic response of channels and floodplains to flooding reflects interactions of erosive and resistive forces with sediment transport capacity and supply at multiple scales. Monotonic relationships between reach-scale response to floods with independent variables such as flood stream power and channel confinement can be confounded by longitudinal variations in these variables at longer scales. In these cases, channel response depends on both local and upstream drivers. Using high resolution pre- and post-flood digital elevation models, we calculate reach-scale (0.5 to 1 km) and segment scale (10 km) longitudinal variations in channel widening and sediment balance. We relate these responses to longitudinal variations of unit stream power and channel confinement for selected streams impacted by the 2013 Colorado Front Range regional flood event. These streams transition from steep and relatively confined in the canyons of the foothills to less steep and unconfined on the high plains. The channel widening response is more closely linked with reach scale gradients in unit stream power: abrupt widening typically occurred within reaches where a large drop in unit stream power occurred relative to upstream. Sediment balance followed segment scale trends in unit stream power, exhibiting a net erosional trend within the foothills that switches to a net depositional trend within the transition to the plains. These findings indicate that unit stream power gradients mediate channel response at reach to segment scales. Predictive modeling of stream response to floods and fluvial hazards assessments that only consider absolute values of reach-scale stream power may under-estimate fluvial hazards in some settings by ignoring unit stream power gradients. © 2018 John Wiley & Sons, Ltd.

KEYWORDS: flood hazards; geomorphology; stream power

Introduction

The relationship between magnitude of geomorphic response to floods and the driving and resisting variables that mediate this response has proven challenging to predict in a quantitative manner. Channels and floodplains respond to floods in complex ways involving vertical and lateral erosion and deposition. These processes are mediated by the hydraulic erosivity of the flood event; the erodibility of the channel, floodplain, and valley margins; and the balance between upstream and local sediment supply and transport capacity. Flood erosivity is a function of discharge magnitude, channel and valley slope, and confinement of the channel by the valley margins (Nanson and Croke, 1992). The caliber and cohesivity of the channel and floodplain sediment, the density and character of vegetation along channel banks and floodplain surfaces, and the composition and slope of valley margins all influence erodibility. Erosivity and erodibility both influence the supply of sediment a stream receives and is able to transport downstream during a flood event. Additional sediment contributed to a stream may be derived from uplands via overland flow and debris flows. Longitudinal variability between sediment supply and transport capacity also play a role in geomorphic response to floods (Gartner *et al.*, 2015).

The first predictive frameworks linking geomorphic response with drivers relied upon qualitative relationships with a single hydraulic variable such as total stream power or stream power normalized by channel or valley width: unit stream power (ω) (Graf, 1983; Miller, 1990; Magilligan, 1992; Costa and O'Connor, 1995). With the rise of geospatial information systems and high-resolution data such as digital aerial imagery and LiDAR-derived digital elevation models, additional variables have been identified as mediating geomorphic response to floods. These include channel confinement by valley margins, degree of coupling with hillslopes, channel radius of curvature, and presence of vegetation along the channel among others (Nanson and Croke, 1992; Buraas *et al.*, 2014; Nardi and Rinaldi, 2015; Fryirs *et al.*, 2016). With these new data, more quantitative predictions based on these relationships are now possible. Researchers can evaluate channel response to floods and a host of other variables that mediate it on both larger (Buraas *et al.*, 2014; Rinaldi *et al.*, 2016) and smaller scales (Lea and Legleiter, 2015; Tamminga *et al.*, 2015) than previously possible. This, in turn, allows for large spatial datasets characterizing geomorphic response to floods with the potential for a better understanding of the relationship between geomorphic response to floods and its drivers.

Recent work has been conducted focusing on predicting the location and magnitude of channel response to floods (Aggett and Wilson, 2009; Krapesch *et al.*, 2011; Vocal Ferencevic and Ashmore, 2012; Buraas *et al.*, 2014; Nardi and Rinaldi, 2015; Parker *et al.*, 2015; Yochum *et al.*, 2017) with the aim of better characterizing (i.e. mapping) fluvial hazard zones and informing the management of infrastructure in stream corridors (Piégay *et al.*, 2005; ASFPM, 2016). These studies often rely on ω as a primary variable in predicting channel response metrics like widening, sediment flux, or response severity class. Mechanistic modeling relating hydraulic variables such as ω or bed shear stress at flood discharges to observations of channel response may improve our ability to predict the magnitude and location of flood response (Aggett and Wilson, 2009; Gartner *et al.*, 2015; Tamminga *et al.*, 2015). However, the predictions may be limited at small spatial units of analysis (Lea and Legleiter, 2015; Tamminga *et al.*, 2015). Consideration of appropriate mechanisms and scales is important in predicting channel response to floods and was achieved well by Gartner *et al.* (2015) who provide a quantitative and mechanistic framework for relating estimates of sediment flux resulting from various flood events to longitudinal variation or gradients in stream power at reach (0.5 to 1 km) and segment (1 to 10 km) scales. Though the linkage between these two variables is presented qualitatively, the patterns are clear and predictable. Sediment flux gradients as a driver of channel adjustment to floods and not just a response is understood to be important, but had not been thoroughly studied due to lack of adequate data.

Other studies have documented that erosive and depositional forms and responses to large flood events correlate with longitudinal variations in ω and channel confinement, defined as the ratio of valley bottom width to channel width. For example, Wohl (1992), Cenderelli and Wohl (2003), Hauer and Habersack (2009), and Thompson and Croke (2013) all found that erosive responses dominated in steeper, confined reaches and depositional responses dominated less confined and milder sloped reaches in both alluvial and bedrock streams. In a hydraulic modeling study, Miller (1995) found that the greatest erosional forces associated with valley morphology occurred at valley expansions. Though not a flood response study, Parker *et al.* (2015) found that the ratio of up to downstream ω, a metric of ω gradient, predicted erosion- vs deposition-dominated segments at the 1–10 km length scale. Lea and Legleiter (2015) and Tamminga *et al.* (2015) found weak relationships between ω and channel response to floods at smaller scale units (50 to 100 m), although these studies did not consider relationships over longer scales. In the present study, we evaluate the ability of ω gradient and channel confinement metrics to predict quantitative channel response metrics over reach (~ 1 km) to segment (~ 10 km) scales.

Along with ω, channel confinement by resistant valley or terrace margins has been thought to play a dominant role in channel and floodplain morphology and adjustability (Nanson and Croke, 1992; Brierley and Fryirs, 2005; Fryirs *et al.*, 2016). Channel confinement acts as a primary influence on channel response to floods by limiting lateral adjustment and eliminating or minimizing floodplain presence. Such floodplains distribute flood waters over wider areas, resulting in opportunities for sediment deposition and associated geomorphic response (i.e. channel avulsion, lateral migration, and braiding; Fryirs *et al.*, 2016).

Though broadly transferable methods for quantitative prediction of channel response to flooding are not described in the literature, modeling frameworks and thresholds for predicting channel change have been developed. These include monotonic relationships evaluated with linear regression models to predict continuous response variables, such as channel widening (Krapesch *et al.*, 2011; Nardi and Rinaldi, 2015; Surian *et al.*, 2016); binary categorical response variables modeled using logistic regression (e.g. single thread or braided channel, Bledsoe and Watson, 2001); as well as ordinal thresholds and categorical response variables modeled using a cumulative logit framework (Yochum *et al.*, 2017). Predicting patterns of channel response and predicting qualitative response variables has proven fruitful and can provide actionable results for floodplain management (Gartner *et al.*, 2015; Yochum *et al.*, 2017); however, our ability to quantitatively predict the absolute magnitude of geomorphic response variables remains limited.

In a companion paper (Yochum *et al.*, 2017), we characterized the ability and limitations of stream power thresholds for predicting ordinal categories of channel response at the reach scale (~ 500 m). We also identified the importance of other variables and subsequent processes that influence channel response, such as local stream power gradient and channel confinement. In the present study we further this line of inquiry by focusing on the role of longitudinal patterns of unit stream power, stream power gradient, and channel confinement in mediating quantitative metrics of geomorphic response: the channel widening response and the volume of erosion and deposition of sediment. Specifically, we:

1) characterize longitudinal patterns of channel response (channel widening and erosion and deposition) at multiple scales, over multiple watersheds and valley types;
2) evaluate which driving variables most influence channel response at different scales; and
3) identify where within a watershed major channel adjustment can be expected from a flood based on the above relationships.

The result of this study is a semi-mechanistic and semi-quantitative framework for evaluating reach- and segment-scale geomorphic response to floods where sediment supplies during floods and gradients in channel slope and confinement are large.

Data and Methods

Study area

From September 9–16 2013, an exceptional amount of precipitation fell along the Colorado Front Range within a corridor nearly 250 km in length, with periods of high intensity rainfall from September 11–13. Maximum depths greater than 450 mm – in excess of average annual rainfall depths for the region – were recorded over the foothills north of Denver resulting in extreme and widespread flooding in over a dozen stream basins (Gochis *et al.*, 2015). Large flood flow magnitudes and durations resulted in extensive geomorphic work (cf. Costa and O'Connor, 1995). Estimates of peak discharge annual exceedance probabilities in the primary flood-impacted areas ranged from 25% to < 0.5% (25 to > 200-year recurrence intervals, Yochum *et al.*, 2017). Over 1000 debris flows were documented in the foothills (Coe *et al.*, 2014), many of which delivered hillslope debris and sediment directly to flooding creeks and streams to be transported downstream (Anderson *et al.*, 2015; Rathburn *et al.*, 2017). The floods initiated in steep and confined streams within the foothills and transitioned to unconfined settings within the plains downstream. Major geomorphic change within stream corridors resulted, concentrated within the foothills and along the transition to the plains.

Our study area lies within the foothills and high plains along the Colorado Front Range. Upper reaches within the foothills run through canyons composed of granite, granodiorite and biotite gneiss, which transition to partially-confined alluvial valleys set within sandstone and shale formations. These give way to alluvium in the plains (Green, 1992). All study reaches lie downstream of the Front Range 'knickzone', a steep region demarking the front of bedrock incision migrating upstream over geologic timescales (Anderson *et al.*, 2006). Downstream of the knickzone, canyon and valley walls are typically steeper than those above the knickzone resulting in a greater susceptibility of landslides and debris flows (Anderson *et al.*, 2015).

We consider the relationship between hydraulic variables describing the erosive power of the floods as well as the reach- to landscape-scale geomorphic setting. We then relate these variables to various metrics measuring physical channel response. These data are collected in a sample of flood-affected watersheds: the Big Thompson River (BT), including a portion

of the north fork, Saint Vrain Creek (SV), including the middle and south forks of Saint Vrain Creek, the North Fork of Saint Vrain Creek (NSV), and Left Hand Creek (LH) including James and Little James Creeks (Figure 1, Table I). Not all watersheds within the footprint of the September 2013 rain event were impacted equally, though our study watersheds contain some of the largest geomorphic changes documented from this event. Within the study area, rainfall was concentrated over the foothills. Discharge peaked near or at the outlet of the canyons to the foothills where the rate of increasing drainage area in the downstream direction begins to decrease and where flood waters are able to spread out over unconfined floodplains and attenuate. The drainage areas of the study reaches range from 20 to 1500 km^2 and slopes range from 0.003 to 0.08 m/m. Our study basins are similar to each other in that the study reaches within them begin in steep, confined canyons of the foothills and transition to the unconfined, more mild-sloped reaches of the plains. We begin and end the geographic scope
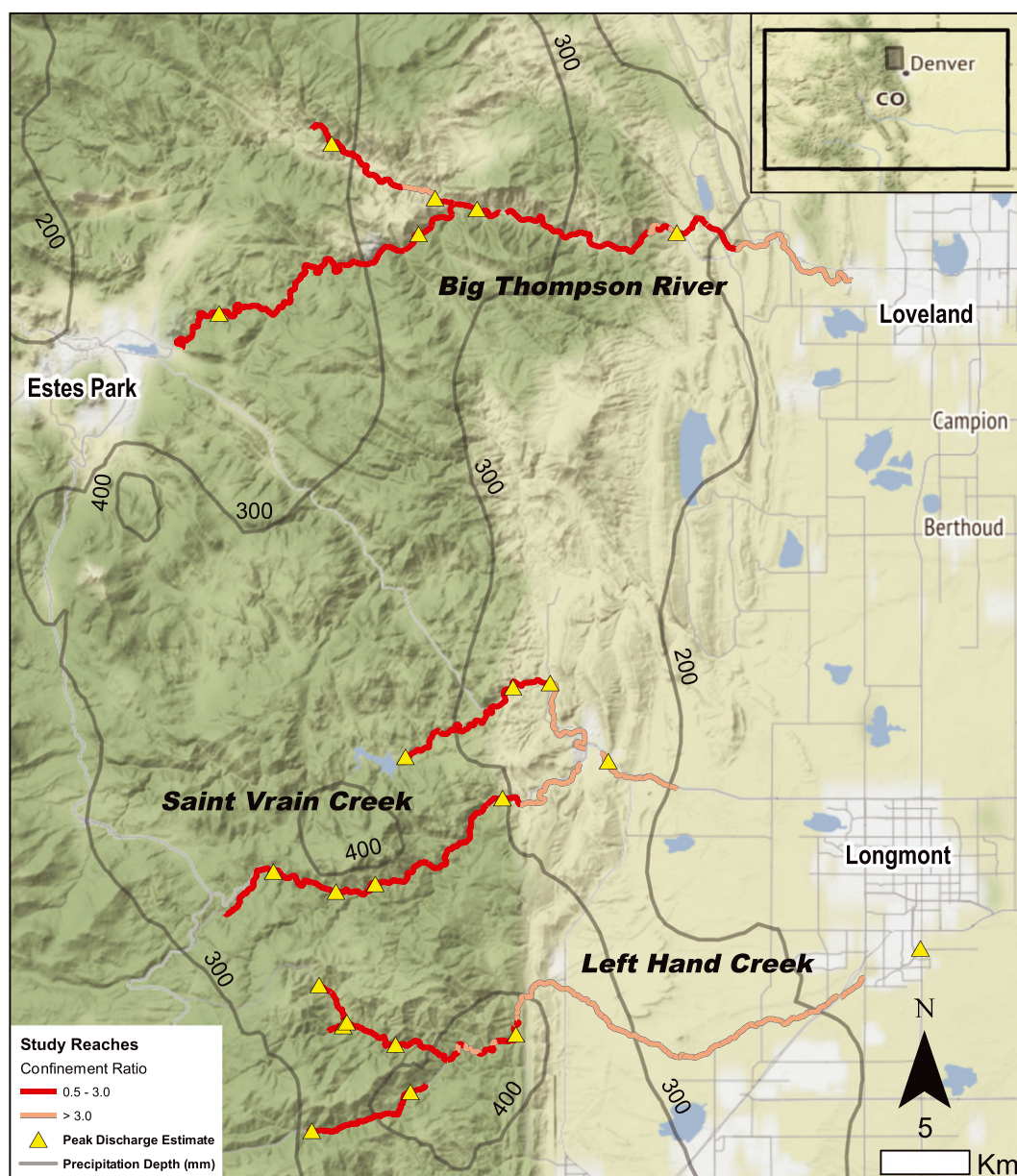

Figure 1. Overview map of study area with confined study reaches in red and unconfined reaches in orange, peak discharge measurement locations in yellow and cumulative rainfall total isohyets in dark gray with precipitation depths in mm. Inset map shows study area within Colorado, USA. Precipitation depths were estimated with the Storm Precipitation Analysis System through a collaborative effort by Applied Weather Associates, LLC, MetStat, Inc. and the Colorado Climate Center. Radar data were supplied by Weather Decision Technologies, Inc. [Colour figure can be viewed at wileyonlinelibrary.com]

Table I. Study area geographic and flood related information by sub-basin. Adapted from Yochum *et al.* (2017)

Watershed	Stream	Length (km)	Number of reaches	Debris flow density (#/km^2)	Drainage area (km^2)	Slope range (m/m)	Peak discharge (m^3/s)	Flood recurrance interval (yr)	Unit stream power (W/m^2)
Big Thompson R.	N. Fork Big Thompson R.	8.4	15		190-220	0.01-0.05	167-272	> 100	300-6700
	Big Thompson R.	42.6	58	0.04	430-1500	0.003-0.065	263-538	100	100-7500
St. Vrain Ck.	N. Fork St. Vrain Ck.	15.0	22	0.04	260-320	0.008-0.03	283-385	-	200-4300
	S. Fork St. Vrain Ck.	22.7	41		170-240	0.01-0.07	50-264	-	200-8000
	St. Vrain Ck.	4.2	7	0.50	560-570	0.007-0.01	699	>200	100-900
Left Hand Ck.	James Ck.	8.8	21		23-48	0.03-0.08	51-122	-	1000-2900
	Left Hand Ck.	31.9	66	1.27	46-180	0.004-0.06	38-199	> 200	100-4600

of our analyses based on the extent of available data, which is typically limited by the availability of peak discharge estimates. As such, the upstream and downstream analysis extents vary from watershed to watershed in terms of drainage area and distance downstream from the continental divide.

We divide the study reaches into two major landscape units (Brierley and Fryirs, 2000): foothills and plains. Foothills reaches tend to be much steeper and more confined than plains reaches. Within the foothills the 1st and 3rd quartiles of reach-averaged slope span 0.02 to 0.036 and those of the confinement ratios (valley floor width/channel top width) span 1.2 to 2.3. Areas of less confinement – floodplain pockets – exist within the foothills, usually at and downstream of major confluences as well as within sharp meander bends within the canyons. Foothills reaches transition to partially confined reaches in alluvial valleys formed within less-resistant sedimentary units. Entering the plains, the 1st and 3rd quartiles of slope for these reaches span 0.007 to 0.013 m/m and those of the confinement ratio span 6 to 29.

Floods along the Front Range below an elevation of approximately 2300 m are dominated by two distinct types of flood events: frequent, less intense snowmelt flooding; and infrequent and intense rainfall-driven floods (Jarrett and Costa, 1988). The latter typically occur in the late summer and fall, though rain-on-snow flood events sometimes occur in the spring. High-intensity, rainfall-driven floods tend to result in greater and more damaging geomorphic change than snowmelt-driven floods but also tend to be more localized. The 2013 flood was an exception to the typically isolated geographic scale of late summer floods and resulted in intense rainfall in many watersheds well above 2300 m in elevation.

Reach delineation

We evaluated geomorphic, hydraulic, and channel response metrics at the reach scale. Reaches were delineated manually and comprise geomorphically-distinct stretches of stream with relatively uniform slope, confinement, and flood response following the concepts of Rinaldi *et al.* (2013). Reach lengths range from 150 m to 1300 m and average 575 m. Our study includes 230 reaches totaling 133 km in length. Values of all hydraulic and geomorphic variables were assigned to the midpoint of each reach for longitudinal analyses.

We did not include segments of stream that were abutted on both sides by bedrock canyon walls and lacked visible alluvial margins (i.e. non-deformable) as well as reaches in the plains whose response to the flood was altered by substantial floodplain encroachment (such as gravel mining operations). Avulsions, erosion, and deposition responses were substantially

influenced in these areas resulting in an incompatibility in reach response between these reaches and those upstream. We did include segments of stream adjoining rip-rapped road embankments in confined reaches that shared the valley floor with roadways. In many cases this rip-rap failed and roadways were washed out, but this bank armoring probably limited lateral channel response in other cases. Small levees and armored banks also existed along some plains reaches. Given the variability in the geographic extent of peak discharge estimates and of the floodplain encroachment along the plains reaches, our analysis extends varying distances from the canyon outlets into the plains for each watershed (10–30 km). Our analysis of NSV ends at the confluence with SV and SV ends at the first gravel pond downstream of this confluence. We end the analysis of BT at the first gravel pond encountered downstream as well. Our analysis of LH extends much further into the plains due to a lack of gravel mining, ending just upstream of where it becomes channelized and enters a fully urbanized area.

Channel confinement

Channel confinement was evaluated by taking the ratio of valley bottom width to pre-flood channel top-of-bank width (Wohl, 2010). Pre-flood top-of-bank widths were sampled for each reach using LiDAR-derived hillshade images and aerial photography. Within the foothills, the majority of reach-scale valley bottom width estimates were generated from a GIS-based tool relying on a 10 m digital elevation model (DEM) (Carlson, 2009). Where this data product was not available, valley bottom width was estimated by identifying the toe of the valley or lowest terrace wall within cross sections cut from pre-flood LiDAR-derived DEMs, which we defined as the 'valley bottom margin' (Fryirs *et al.*, 2016). An average of five channel width and valley cross-section measurements were collected for each reach. We defined confined channels as those having confinement ratios ≤3, and unconfined channels with ratios > 3. This threshold categorizes semi confined reaches within the foothills (i.e. floodplain pockets) as unconfined. Creating an intermediate confinement category (e.g. 3 < confinement index ≤ 7) did not add to this study as these reaches behaved similarly to those with a confinement index > 7.

Channel confinement largely tracked with landscape unit: confined channels were mostly located within the foothills region, less confined channels in the wider valleys immediately downstream of the canyons in the transition to the plains, and unconfined channels were located within the plains region. Confinement and slope tend to track together as well: average channel slope is greatest for confined channels and is smaller for unconfined channels.

Unit stream power

Peak unit stream power ω (W/m^2), defined as total stream power Ω (W/m) normalized by post-flood channelized flow width, w, is estimated as the product of the specific weight of water, γ, peak discharge, Q, and channel slope, S, divided by w:

$$\omega = \gamma Q S / w \qquad (1)$$

Channelized flow width was defined by the post-flood width measured between discernable tops of channel banks (i.e. top-of-bank width). Peak discharge values were compiled from several sources by Yochum *et al.* (2017) using a variety of methods described in Moody (2016). In some cases, multiple independent estimates were co-located for comparison. In cases of disagreement, we chose the estimate that provided for the best continuity of increasing discharge in the downstream direction within the foothills, or decreasing in peak discharge due to floodplain attenuation in the plains (e.g. LH). Peak discharge values were linearly interpolated using distance between two measurements that lacked major intervening tributary inputs. Reaches were excluded from analysis below confluences downstream of which a measurement was lacking. Nevertheless, a high density of peak discharge estimates along the Front Range provided for a continuous set of peak discharge estimates in our study basins (Figure 1).

Channel discharge values were estimated from the total peak discharge values for confined reaches. In unconfined reaches with substantial floodplain flow, the portion of the flow within the channel used to estimate ω was evaluated using a one-dimensional hydraulic model (HEC-RAS v.4.1). Hydraulic models were created from post-flood LiDAR-derived digital elevations models. See Yochum *et al.* (2017) for more details on the hydraulic modeling methods. A reach averaged slope was calculated using the elevations at the up- and downstream ends of each reach sampled from a pre-flood LiDAR-based DEM. Therefore, reach-scale ω estimates are not based on a uniform length scale as reach lengths are not uniform.

Unit stream power gradient is represented as the ratio of downstream to upstream ω calculated from adjacent reaches:

$$\omega_r = \omega_{DN} / \omega_{UP} \qquad (2)$$

where ω_{DN} is the value of reach-average ω on a downstream reach and ω_{UP} is the value of ω for the adjoining reach upstream. This ratio indicates where a positive ($\omega_r > 1$) or negative ($\omega_r < 1$) gradient exists for reach scale ω (Parker *et al.*, 2012). Net erosional and depositional reaches correlate well with gradients of ω (Parker *et al.*, 2012; Gartner *et al.*, 2015). Reaches with ω_r values within ± 0.1 of unity were removed from analyses where this metric was used to classify reaches as having positive or negative ω gradients.

Erosion and deposition

Reach-scale erosion and deposition within the stream corridor was estimated using DEMs-of-difference (DoDs) calculated from 0.75m resolution DEMs generated from LiDAR data collected by third party agencies. A 2011 LiDAR flight was performed over SV and LH, a spring 2013 pre-flood flight was performed over BT, and a 2013 post-flood flight was performed over all watersheds. Streams were at low base flow conditions during pre-flood LiDAR data collection. Post-flood LiDAR was collected in October 2013 when streams were under elevated base flow conditions. These data were obtained from the State of Colorado via <https://geodata.co.gov>. Digital Elevation models were

not corrected to account for water depth before performing the difference calculation. Typical ranges of vertical channel change from the flood (1 to 3 m) are considered much greater than differences in water surface elevations within the channel between LiDAR flights (0.1 to 0.3 m). We thresholded the DoDs (*sensu* Wheaton *et al.*, 2010) to remove values that fell within ± two standard deviations of estimated error sampled from areas where no change in elevation was expected. To sample the DoD area along each reach corridor, we hand digitized polygons that extended from valley wall to valley wall and included areas where valley margins were eroded. Our erosion and deposition metric, ΔV, was calculated as the sum of elevation differences within a channel corridor, $Z_{post} - Z_{pre}$, multiplied by the area of that corridor, A, and normalized by the reach length, L:

$$\Delta V = 1000 \cdot A \sum \left(Z_{post} - Z_{pre} \right) / L \qquad (3)$$

The sediment balances reported here are not closed because they start at arbitrary locations within each watershed at the upstream-most extent of data availability and do not account for debris flow inputs. Debris flow occurrences over the 2013 flood mapped by Coe *et al.* (2014) were used to indirectly estimate hillslope sediment supply to the study reaches. Debris flow density per unit watershed area was calculated for each major reach and is reported in Table I.

Fluvial disturbance width

Using a combination of pre- and post-flood high-resolution aerial photography, 0.75 m DEM hillshade rasters, and the thresholded DoD rasters, we measured pre-flood channel widths (W_{pre}) and post-flood fluvial disturbance width (W_{post}) to determine the widening ratio:

$$W_r = W_{post} / W_{pre} \qquad (4)$$

Between 3 and 30 width measurements were collected along each reach and averaged. Pre-flood channel width is an estimate of the channel top-of-bank width. Whereas W_{post} estimates the outer fluvial disturbance width or the outer limits of channel widening and braiding. The definition of W_{post} is an important hazard management consideration and a more accurately delineated feature compared with post-flood channel width in many areas where braiding and avulsion occurred and defined channel banks did not exist. Note that the widening ratio incorporates data from one reach before and after a flood, whereas ω_r incorporates data from a given reach and the reach immediately upstream.

Statistical analysis

We rely on non-parametric tests of differences in median values of channel response metrics among various groupings of categorical predictor variables due to unequal variances among these groups as well as non-normality. As such, we used the Wilcoxon rank sum test for difference in medians using the base stats package in R (R Core Team, 2016). For comparing more than two groups, we used a non-parametric multiple comparisons test following a Kruskal-Wallis test with a critical p-value of 0.05 using the pgirmess package in R (Siegel and Castellan, 1988; Giraudoux, 2016). Quantile regression of W_r and ω_r was performed using the quantreg package in R (Koenker, 2016). Monotonic trend tests were performed using the Kendall τ statistic for heteroscedastic data using the Kendall package (McLeod, 2011).

Results

Longitudinal variability in channel response

In all streams, ω values begin relatively low in the headwaters region reaching a maximum within the middle portion of the foothills (where precipitation maxima were also observed). Unit stream power sharply reduces at the transition from the canyons to alluvial valleys and plains. Large fluctuations in ω are observed within the middle portion of the foothills where steep, confined canyons resulting in local maxima of ω transition to less confined 'floodplain pockets' where confinement and slope decrease resulting in local minima of ω. Here, local widening maxima occur at local ω minima or troughs as well as toes in the downstream ω pattern (Figure 2(A) and Figure 3 (A), BR at river kilometer (RK) 16, 19, and 27). Toes occur in reaches located at the base of large drops in ω, where ω values remain low in the downstream direction for some distance such as in the transition from the canyons to alluvial valleys and plains (e.g. Figure 3(A), BT at RK 32 and SV at RK 19). Note that the values of all reach-scale variables are plotted at the midpoints of each reach in Figures 3 and 4.

The fluvial disturbance width jumps at the transition from the foothills to the plains where confinement and slope (and hence ω) both decrease concurrently within the transition to less confined valleys (Figures 2(B) and 3(A)). In the transition out of the foothills, these valleys give way to the plains where channels are largely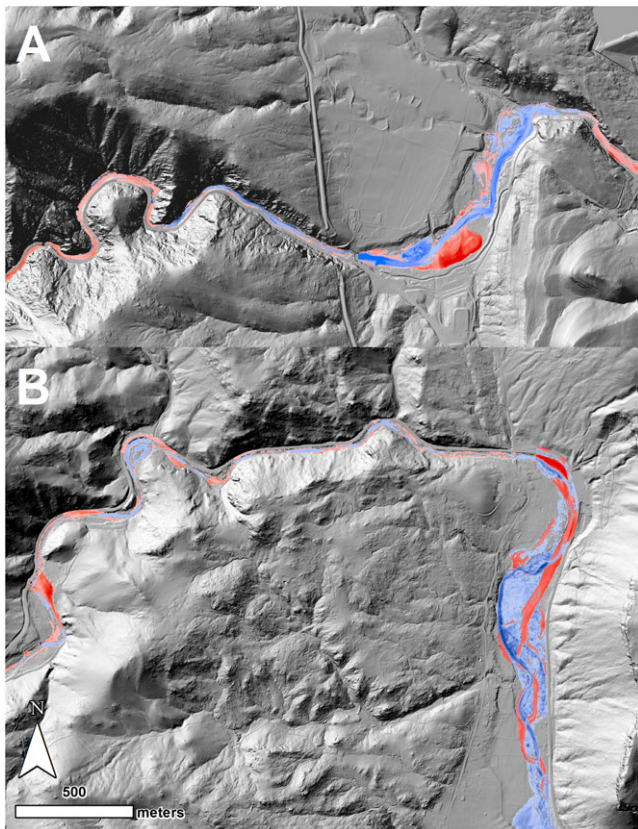 unconfined. In some cases, this jump in channel widening occurs immediately downstream of the outlet of the canyons of the foothills (e.g. BT) denoted as vertical blue lines in Figure 3. In other cases, a lag ranging from 1 to 4 km is observed before a jump in W_r occurs downstream of the canyon outlets (Figure 3(A), NSV, SV, and LH). Elevated W_r values continue downstream for 3 to 8 km before declining again. In the plains region, W_r is high but oscillates from reach to reach due to cycles of channel avulsion and then re-concentration of flow in the original channel (Figure 3, LH, NSV, and SV; Figure 4). In Figure 4, peaks of W_r values coincide or immediately follow troughs in the longitudinal pattern of ω_r, which is potentially driven by reach-averaged slope oscillating between approximately 0.02 and 0.01 m/m. Channel confinement by the valley margin does not vary along this particular stream segment.

Cumulative sediment balance summed longitudinally shows net degradation within the foothills region transitioning to net aggradation in the plains (Figure 3(B)). Steep negative trends in sediment balance are observed for most streams in the middle reaches within the foothills where precipitation was concentrated, slopes are high, and channels are confined, all of which result in large values of ω. This erosional trend changes to a net depositional trend at the outlet of the canyons and in the transition to the plains where slopes are milder, the channels less confined, and ω reduces compared with the foothills. Channel widening and braiding are often associated with this depositional trend within the first approximately 10 km from the canyon outlets.

Though sediment balance appears more responsive to segment-scale rather than reach-scale patterns in ω, locations of punctuated aggradation are observed at or downstream of substantial decreases in ω ($\omega_r \ll 1$). For example, a large step in net aggradation occurred on LH from kilometers 14–15 after a sharp decrease in ω upstream at kilometers 11–12 (Figure 3(B)). Longer lag distances between these two phenomena are observed on BT and SV, while no lag is observed at NSV. On NSV, rapid rates of sediment deposition continue two to four kilometers downstream and then level off. Note that a sharp increase in sediment volume change occurs within the foothills on NSV (RK 2) where a large quantity of sediment filled a run-of-river diversion dam.

Figure 2. Examples of DEMs-of-difference with net degradation in red and aggradation in blue overlain on hillshade images showing channel response at transitions from steep, confined reaches to less steep, unconfined reaches. Direction of flow is west to east. A: BT at transition to floodplain pocket within foothills. B: NSV at transition from confined to alluvial valley reach. In general, net erosional change in surface volume (red areas) in confined reaches give way to a braided channel response with degradation where new channels were formed and aggradation where old channels were filled and floodplain deposition occurred. [Colour figure can be viewed at wileyonlinelibrary.com]

Fluvial disturbance width

Reach-scale W_r appears to be a decreasing function of ω (Kendall $\tau = -0.18$, $p = 3.6E-5$), though heteroscedasticity is noted for this relationship (Figure 5). For confined reaches, W_r is not a significant function of ω ($\tau = -0.09$, $p = 0.1$) and is a weakly significantly decreasing function of ω for unconfined reaches ($\tau = -0.15$, $p = 0.05$). The negative correlation between W_r and ω is probably related to the largest observed ω values occurring in steep, confined reaches within the foothills where widening was geologically limited. Indeed, nearly 68% of confined reaches by length experienced widening that extended from valley margin to valley margin, which in many cases included the roadway embankments (Figure 3(A) and Figure S3 in Supplemental materials). Noise in these relationships can be explained in part by the influence of stream power gradient (ω_r), especially at smaller values of ω for which a wide range of ω_r is observed.

The central tendency of W_r is mediated by ω_r and confinement. Confined reaches have a significantly different median W_r value (1.8 ± 0.1, $\pm$ one standard error of the median, Table II) compared with unconfined reaches (2.3 ± 0.3). Unconfined reaches with negative ω gradient exhibit the largest fluvial disturbance width response with a median W_r value of 3.0 ± 0.4 (Table III). Reaches with negative ω gradients have
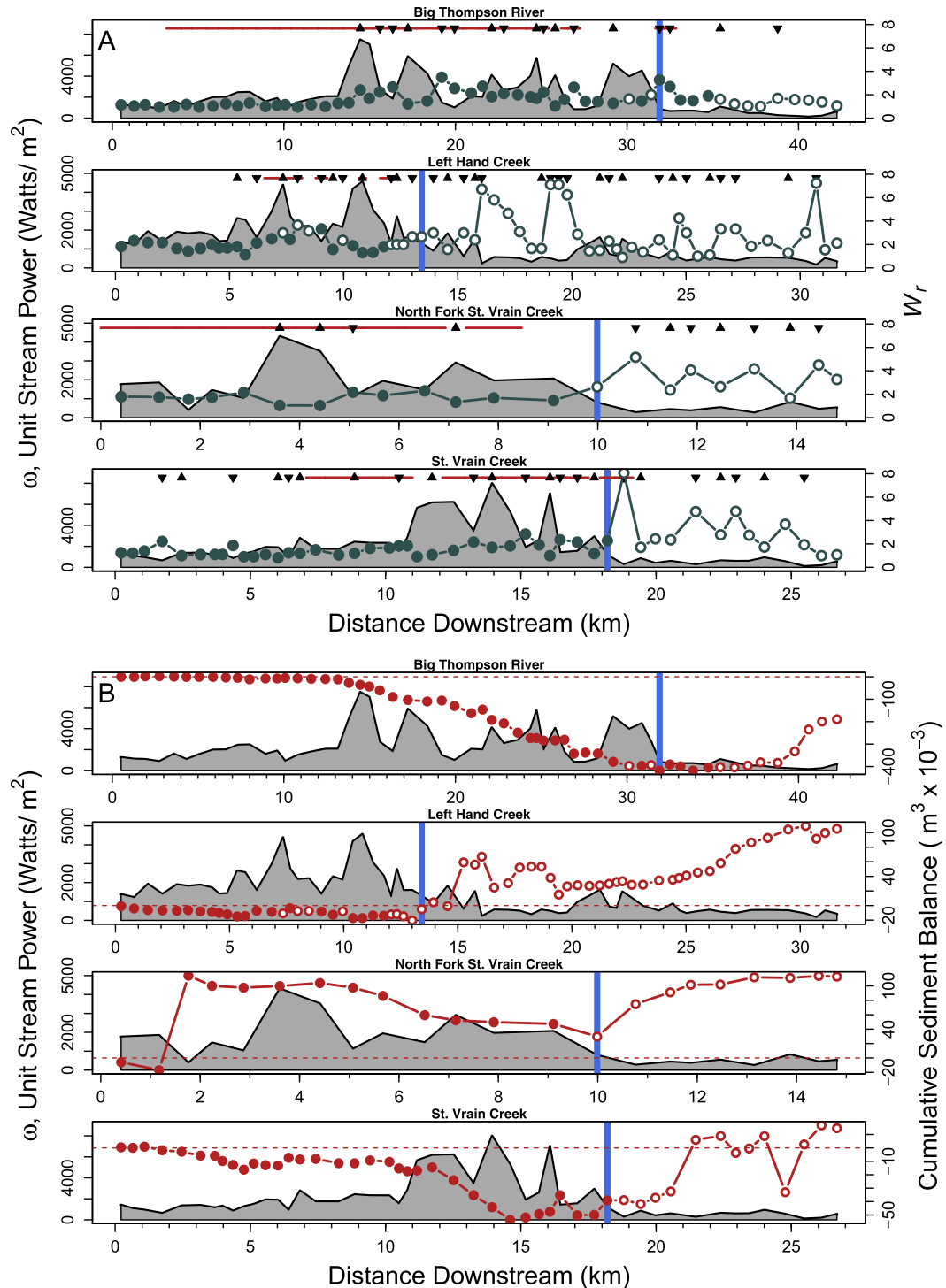
Figure 3. A: Reach scale widening ratio (green lines) plotted over the longitudinal pattern of ω (grey polygons). Open circles indicate unconfined reaches (confinement ratio ≥ 3) and closed circles indicate confined reaches (confinement ratio < 3). Vertical blue line indicates downstream-most extent of confined foothills reaches and transition to plains. Upward-facing triangles denote reaches with peaks in the longitudinal ω pattern and downward-facing triangles denote troughs and toes. Red horizontal lines denote reaches that widened to the valley margins. B: Cumulative sediment balance (red lines) generated from summing reach-scale balance as calculated by DoD's evaluated over the channel and floodplain for each reach and plotted over the longitudinal pattern of ω (grey polygons). Horizontal, dotted lines indicate a cumulative balance of zero. Note that a run-of river diversion dam located at 1.5 km on NSV resulted in a large spike of aggradation within the foothills. [Colour figure can be viewed at wileyonlinelibrary.com]

statistically significant larger W_r regardless of confinement setting, compared with reaches with positive ω gradients (Figure 6(A), Tables II and III).

For $ω_r < 1$ (negative ω gradient), much larger and more variable values of W_r exist in the continuous relationship between W_r and $ω_r$ (Figure 7(A)). Values of W_r are the highest for reaches with the most negative ω gradients found at troughs or toes in the downstream longitudinal pattern of ω compared with all

other reaches (Figure 3(A) and 7(B)). No divergent relationship is observed between W_r and $ω_r$ for unconfined versus confined reaches, though the response for unconfined reaches is more variable. Quantile regressions of the relationship between width ratio and the logarithm of $ω_r$ evaluated at median and 0.95 quantile values indicate a decreasing relationship. The intercepts for both models are significant ($p < 1E-5$ for both) and slope is significant for the median regression model ($p = 9E-5$)
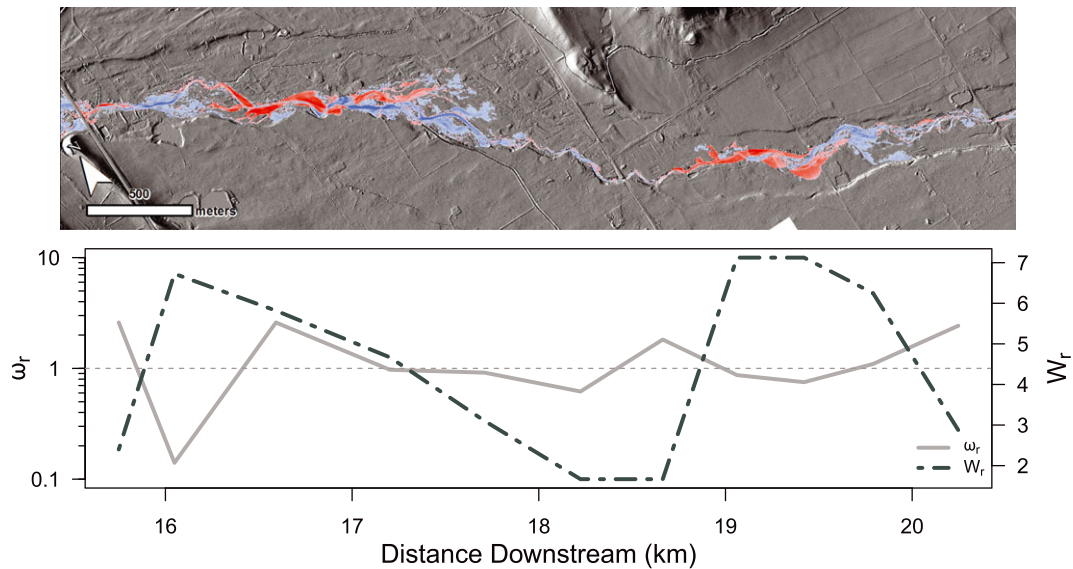
Figure 4. Image of stream segment on LH showing DoD as well as fluvial disturbance width (top). Reach-scale pattern of W_r overlaying longitudinal pattern of ω_r shows an oscillating expansion and contraction of W_r along LH in the plains (bottom). Peaks in ω_r roughly align with areas of greater W_r values and troughs with smaller W_r values. [Colour figure can be viewed at wileyonlinelibrary.com]
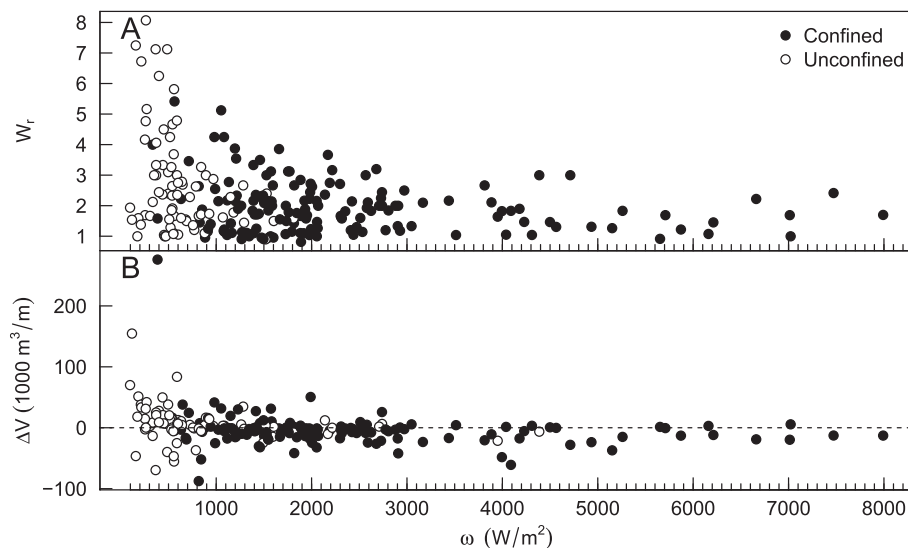

Figure 5. Plots of W_r (A) and ΔV (B) as a function of ω with confined (black) and unconfined (white) reaches identified.

Table II. Results of Wilcoxon Rank Sum test between median values of W_r and a signed rank test between median values of ΔV and zero for stream power gradient and confinement categories

	Median W_r	*P*-value	Median ΔV	*P*-value
$\omega_r > 1$	1.6		−2.1	4.0E-03
$\omega_r < 1$	2.3	4.4E-09	−0.8	0.5
C	1.8		−3.0	1.8E-05
U	2.3	1.3E-05	4.6	1.0E-02

but not the 0.95 quantile model (*P* = 0.14, Figure 7(A)). The 95th quantile regression was performed to quantify an upper envelope of observed width ratio as a function of log10(ω_r).

Erosion and deposition

Net erosion and deposition do not vary systematically with absolute values of ω at the reach scale (Figure 5(B)). Reaches with very large values of ω (> 3000 W/m²) are nearly uniformly erosional and reaches with relatively lower values of ω (<

1000 W/m²) exhibit wide ranges of deposition and erosion. Nor is ΔV very sensitive to reach-scale longitudinal variation in ω (Figure 3(B)). Confined reaches tend to be erosional and unconfined reaches depositional regardless of ω gradient (Table II, Figure 6(B)). This relationship largely reflects the segment scale pattern of net erosion in the foothills, where streams are primarily confined, and net deposition in the plains where streams are primarily unconfined.

Stream power gradient (ω_r) more weakly influences ΔV compared with confinement or landscape unit (foothills or plains, Figure 6(B), Tables II and III). The median value of ΔV of reaches with positive gradients is significantly erosional, whereas the median values of ΔV for reaches with negative gradient is not significantly different from zero (Table III). However, there are notably more confined reaches with positive values of ΔV where $\omega_r < 1$ than there are where $\omega_r > 1$, indicating that stream power gradient plays a role in sediment erosion and deposition patterns even in confined reaches (Figure 6(B)). As with the widening response, reaches with negative ω gradients result in larger variability in ΔV response. Unconfined reaches with negative ω gradients have the widest spread in ΔV response (including some net erosional values). These reaches also demonstrate

Table III. Results of multiple comparisons tests of median values of width ratio and net unit volume change among unit stream power gradient and confinement categories

ω Gradient	Confinement		Width ratio, W_r					Unit volume change, ΔV			
			$\omega_r > 1$		$\omega_r < 1$			$\omega_r > 1$		$\omega_r < 1$	
			C	U	C	U		C	U	C	U
		Median	1.5	1.7	2.2	3.0	Median	-3.0	2.9	-2.7	6.8
$\omega_r > 1$	C	1.5			X	X	-3.0		X		X
	U	1.7				X	2.9				
$\omega_r < 1$	C	2.2					-2.7				X

Note: Median values of W_r and ΔV are provided with units of m/m and $m^3/m \times 10^3$, respectively. X denotes significant differences between pairs.
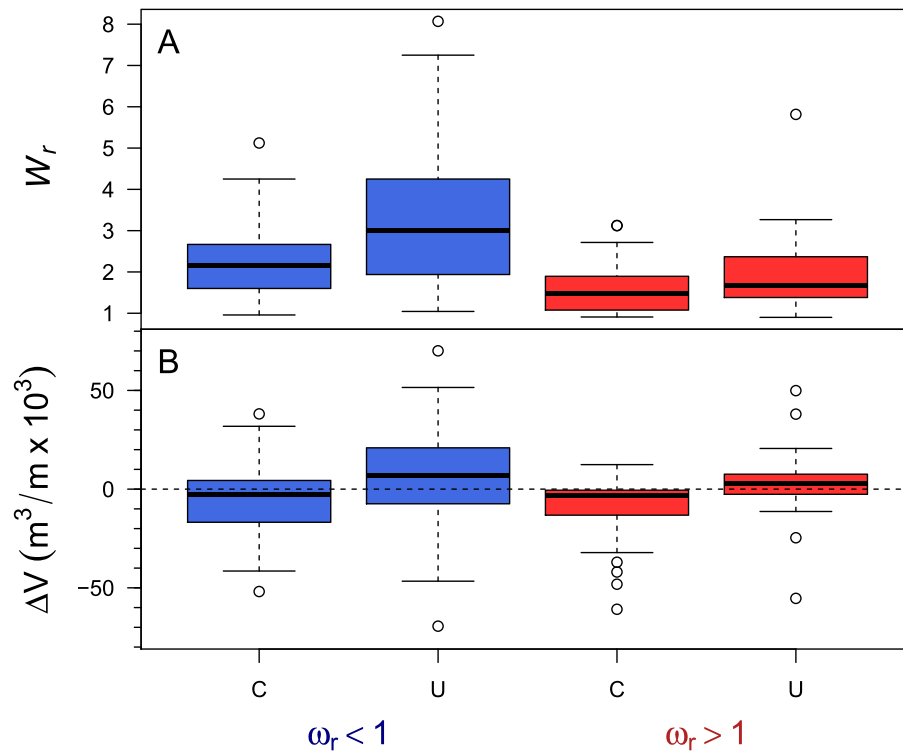

Figure 6. Boxplots comparing widening ratios (A) as well as net volume change normalized by reach length (B) among unit stream power gradient ratio and channel confinement categories: confined (C) and unconfined (U). Negative stream power gradient ($\omega_r < 1$) results in larger and greater variability in W_r values. Median values of volume change are negative for confined and positive for unconfined reaches. Within these categories, reaches with negative stream power gradient tend to have higher median values. [Colour figure can be viewed at wileyonlinelibrary.com]

greater absolute values of net deposition than unconfined reaches with positive gradients.

There was not a detectable relationship between the fluvial disturbance width and erosion and deposition status at the reach scale. We did not find a significant difference in median widening ratios between net depositional versus net erosional reaches ($p = 0.93$). Channel widening can result from erosion of the channel margins, a process that dominated in the foothills region, as well as deposition, a process that dominated in the transitional valleys and plains region. The much larger widening ratios observed in the plains occurs as a result of channel avulsion and braiding responses and lack of confinement by valley margins.

Discussion

Drivers and scale of channel response to floods

The fluvial disturbance width and patterns of erosion and deposition are influenced differently by the independent variables studied and their responses occur over different length scales. Of the variables studied, reach-scale W_r is most influenced by ω_r followed by confinement, whereas reach-scale ΔV is most influenced by confinement followed by ω_r (Figure 6, Tables II and III). Unconfined reaches with negative ω gradients exhibited greater values of W_r and were more depositional than erosional compared with confined reaches with positive ω gradients. Erosion and deposition trends are less sensitive to reach-to-reach variability in ω. Rather, they follow segment-scale trends in ω and confinement from the foothills to the plains with a net erosional trend in the foothills that transitions to a net depositional trend in the plains.

Reach-scale estimates of W_r are sensitive to reach-to-reach scale changes in ω especially at troughs and toes in the longitudinal pattern of ω where negative ω gradients are the strongest and W_r values are the greatest (Figure 7(B), S7). Reach-scale W_r is a decreasing function of ω_r; however, much variability exists in this relationship making ω_r an imperfect continuous predictor of W_r (Figure 7(A)). Rather, ω_r performs well as a categorical covariate used to discriminate between positive and negative ω gradients (Figure 6(A)). The variability in this relationship is
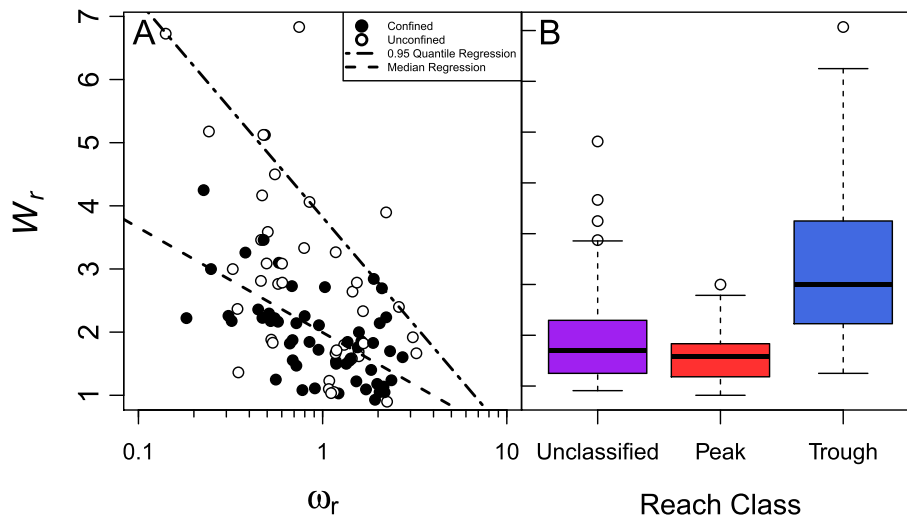
Figure 7. A: Plot of width ratio as a function of log10(ω_r). Open circles are unconfined reaches and closed circles are confined reaches. The x-axis is on a log scale to more equally distribute ratio values greater than and less than unity. Quantile regression lines delineate median and 0.95 quantiles of width ratio as a function of log10(ω_r). Quantile regression line intercepts (b_0) and slopes (b_1) are given along with p-values in Table S2. B: Boxplots of reach-scale widening ratio classified by reach location within longitudinal pattern of unit stream power. Peak reaches are located at unit stream power peaks (i.e., BT: RK 14, Figure 3) and trough reaches are located at unit stream power troughs (i.e., BT: RK 16) or at the downstream toes of drops in unit stream power (i.e., BT: RK 32). Unclassified reaches are the remainder that fall in between peaks and troughs. [Colour figure can be viewed at wileyonlinelibrary.com]

reduced when W_r and ω_r are evaluated over longer reaches encompassing consistent rising, falling, and constant trends of the longitudinal pattern of ω.

Channel widening via erosional processes (bank erosion and hillslope mass wasting) typically occurred in confined channels with very large values of ω (e.g. Figure 3(A), BT: RK 14–20). The widening response in these reaches was smaller compared with unconfined reaches due to geologic constraints of bedrock and colluvial valley margins. Nevertheless, some 68% of confined reaches by length experienced fluvial disturbance across the entire width of the valley. In some discrete areas the valley was widened due to hillslope failure caused by the flood. Widening due to depositional processes (braiding and avulsion) and channel migration typically occurred for unconfined channels with much lower values of ω (e.g. Figure 3(A), LH: RK 15–20). Regardless of confinement, local maxima in the longitudinal pattern of W_r occurred at troughs or toes of ω where the ω gradient is most strongly negative. The majority of these ω trough and toe reaches were erosional in the foothills and depositional in the plains, following the segment-scale trends of ΔV previously noted (Figure S7).

Erosion of lateral channel margins was the primary source of sediment exported downstream in a study on the NSV upstream of our study area, though debris flows were also important contributors of sediment (Rathburn *et al.*, 2017). Though the longitudinal sediment balances reported in Figure 3(B) are not complete, the surpluses of sediment seen in several streams (LH, NSV, SV) indicate that sediment supplied from hillslopes via debris flows and landslides augmented the supply of sediment in transport beyond what was eroded from channel margins (Anderson *et al.*, 2015). The large coarse sediment loads associated with this flood event played a large role in geomorphic response to the floods within the alluvial valley and plains reaches.

Both the magnitude and gradient of ω are important mediators of channel response. Yochum *et al.* (2017) presented ω thresholds for categories of geomorphic response to floods (monotonic relationships between channel response and ω) and noted that these apply to segments of stream where channel confinement and ω gradient are relatively uniform. Where substantial transitions of channel confinement and

slope exist along a stream, monotonic relationships between ω and channel response tend to not hold. Yochum *et al.* (2017) did not investigate W_r as an explanatory variable, but rather evaluated geomorphic adjustment based on a semi-quantitative visual assessment of change using ordinal categories of response. Unit stream power peaked in the canyons of the foothills where bedrock and colluvial valley margins confined the channels and limited W_r values. There we documented many reaches in which the fluvial disturbance width extended to the valley margins (Figure S3). These two factors help explain the seemingly decreasing relationship between W_r and ω (Figure 5(A)). Normalizing W_r values by valley width or considering the ratio between valley width and pre- and post-flood channel width might improve the comparison of fluvial disturbance width between confined and unconfined reaches.

The interaction between stream power, stream power gradient, confinement, and channel response to floods has been observed extensively (Wohl, 1992; Cenderelli and Wohl, 2003; Hauer and Habersack, 2009; Thompson and Croke, 2013; Nardi and Rinaldi, 2015; Surian *et al.*, 2016). Nanson and Croke (1992), use confinement along with stream power and grain size as dominant variables in floodplain and disturbance regime classification (i.e. response to floods). By definition, less confined reaches have more degrees of freedom to adjust than confined reaches because less of their length is in contact with resistant valley margins and are therefore more responsive to a variety of disturbances, including floods (Fryirs and Brierley, 2010; Fryirs *et al.*, 2016).

In the companion study, channel confinement ratio and category (i.e. confined and unconfined) were significant predictors of ordinal channel response category (Yochum *et al.*, 2017). There, we found that for a given values of ω, a more severe channel response was generally observed in unconfined vs confined channels. This relationship is observed in the present study as well (Figure 5). Fryirs *et al.* (2016) distinguish confinement of channels by contact with resistant margins and channel constriction. Both aspects of confinement are at play in channel response in our study. Less resistant boundaries along reaches within the alluvial valleys and plains allowed for a more extreme widening response and a sudden reduction in channel

Qualifications and knowledge gaps

In this study, we focus on metrics of channel confinement and stream power gradient as primary predictors of channel response. We do not emphasize quantitative linkages between the independent and response variables we studied due to the large uncertainty in the relationships (i.e. Figure 7(a)). Rather, we focus on the qualitative patterns and statistically significant differences between response variables and categories of independent variables (Tables II and III). Though statistically significant, much scatter exists in the relationships we report implying that other variables not quantified in this study also play a role in channel response.

Boundary resistance, an important variable in channel response, was not evaluated. The influence of vegetation, bed and bank armoring, and the inherent resistance of boundary materials due to size or composition were also not evaluated. Most similar studies do not explicitly account for boundary resistance either (Surian et al., 2009; Krapesch et al., 2011; Gartner et al., 2015). Nardi and Rinaldi (2015) did consider the influence of percentage of vegetated banks on channel widening. They found that the presence of vegetation did not reduce channel widening response and may have enhanced it in some cases with the hypothesis that flow resistance from vegetation may aid in deposition and avulsion responses during floods. The overall lack of characterization of boundary resistance in flood response studies is a shortcoming of this type of study and reflects the more field intensive nature of defining resistance variables such as bed and material sampling and characterizing vegetation density. Surficial geology maps, which can inform boundary material composition, are readily available though at coarse scales (Green, 1992). Riparian vegetation may also be mapped using remotely-sensed data as in Nardi and Rinaldi (2015), though the limited resolution of these data make them hard to employ for small streams and in confined settings like the foothills of the Colorado Front Range.

Resistant granite and associated colluvium form the lateral boundaries of the majority of confined channels in the foothills (Green, 1992). Pockets of partially-confined reaches contain stores of more erodible alluvium. Moving downstream to the partially-confined alluvial valleys, which are set within sandstone and shale formations along with alluvium, and the plains, dominated by alluvium, lateral resistance to erosion decreases. The increased channel response observed in alluvial valley and plains reaches may in part be due to this reduction in lateral resistance to erosion. The reduction in sediment transport capacity and subsequent deposition of sediment in transport also played a large role in mediating channel response in these areas.

Sediment inputs to the study reaches during the flood include the channel and valley margins, measured in the ΔV calculations, as well debris flows, which were not evaluated. Nevertheless, inputs from debris flows may have influenced channel response at the site of and downstream of these. In a study of 120 debris flows resulting from this flood, Anderson et al. (2015) did not observe widespread evidence of debris fans below debris flow runouts. Rathburn et al. (2017), found that landslides and debris flows on hillslopes accounted for approximately 40% of sediment eroded in the upper North Fork St. Vrain Creek watershed, which is located entirely within the foothills, and channel margins contributed the remaining 60%. Nearly 60% of this sediment was delivered to a downstream reservoir and 40% was stored in channel margins that had widened as a result of the flood. Both of these studies indicate that the majority of debris flow supplied sediment was transported downstream during this flood event. We did not find a strong relationship between density of debris flow events and geomorphic response at the scale in which we conducted our observations. Large point inputs of sediment to a stream likely do enhance channel response at the source and for some distance downstream. Debris flows also amplify the volume of runoff as well as its density, potentially increasing the erosive energy of the flood (Kean et al., 2016). The relationship between point sources of sediment from debris flows and channel flood response, as well as the role of sediment flux on channel response is a ripe area for further research.

Finally, we evaluated reach-averaged values of ω based on our manually-delineated, geomorphically-distinct reaches. These reaches did not have uniform lengths because we delineated reaches within relatively homogenous valley types, adjacent land uses, and geomorphic responses to the flood. Elsewhere, ω has been evaluated as a continuously-sampled variable over uniformly-spaced intervals (Gartner et al., 2015; Lea and Legleiter, 2015). Gartner et al. (2015) discuss the importance of choosing an appropriate length scale for smoothing ω values to better discern longitudinal trends. We lumped reaches that were part of segments of continuous longitudinal ω trends (increasing, flat, decreasing) to evaluate how averaging ω and channel responses over longer distances would influence the results. This lumping exercise resulted in largely similar results to not lumping in terms of the longitudinal relationships between channel response metrics and ω (Figure 4) along with the influence of ω gradient and confinement on channel response metrics (Figure 6).

The accuracy of predicting channel response to floods using similar metrics has been demonstrated to increase with the scale of analysis domain. Poor relationships have been observed between channel response metrics and stream power metrics at smaller scales (60 m) (Lea and Legleiter, 2015) and within individual reaches (Tamminga et al., 2015). Clearer relationships were found between stream power gradient metrics averaged over longer reach scales and erosion and deposition responses (100 to 1000 m: Gartner et al., 2015; 1 to 10 km: Parker et al., 2015) and channel widening responses (10 to 50 km: Krapesch et al., 2011). In the present study, the variability in the decreasing relationship between W_r and ω_r decreased when variables were averaged over longer reaches within similar increasing, decreasing, and steady longitudinal trends of ω.

Applications

We observed a maximum W_r of 8.0 in the plains and 5.6 in the foothils study. The largest W_r value within the plains occurred in an unconfined reach with relatively mild slope and a strongly negative stream power gradient (Figure 3(A), SV: RK 19, $\omega_r = 0.23$). Here, downstream channel migration and avulsion contributed to the large width of disturbance. Channel widening ratio is a decreasing function of ω_r, and is typically lower in confined reaches. A wider hazardous zone may exist along reaches with values of ω_r that are much lower than unity, low absolute values of ω, and lack of confinement. These reaches are typically located at troughs or toes in the downstream longitudinal pattern of ω, located in floodplain pockets within the foothills and in the alluvial valleys immediately

downstream of the foothills within the transition to the plains. However, steep, confined reaches have their own hazards. In many cases W_r was limited by bedrock valley margins and streams widened to occupy the entire, albeit narrow, width of the valley bottom (including paved roads with armored embankments). Nearly 68% of these reaches by length experienced fluvial disturbance that extended across the entire valley (Figures 3(A) and S3). Channel incision and subsequent hillslope mass wasting along with the erosion of channel margins all contribute to highly hazardous fluvial environments in steep, confined reaches.

Large increases in channel widening began zero to four kilometers downstream of the canyon outlets and continued to be high, though oscillatory, for two to eight kilometers downstream. The downstream length of widening response on the Big Thompson River was notably less than the other study reaches. This is likely not explained by a difference in upstream sediment supply as much sediment was eroded from the valley bottom upstream on this stream. Rapid sediment deposition began from zero to eight kilometers downstream of canyon outlets and continued for two to six kilometers. Reach-scale widening and sediment deposition are not coupled as elevated widening typically began closer to canyons outlets and the net depositional trend began further downstream. At the canyon outlets, ω decreased due to milder slope and wider floodplains even though flood discharges generally peaked just upstream and attenuated as the flood moved downstream through the plains. Rainfall was concentrated over the foothills for this flood event. Greater rainfall over the plains might have extended this zone of elevated widening and deposition farther downstream by providing enchanced transport capacity within plains reaches.

In Figure 8, we present a conceptual model of generalized channel response to floods, in terms of W_r and ΔV, as one moves from the foothills to the plains. In the foothills, channel widening and bed incision produce a net erosional response over segment length scales. Channel widening can influence the entire valley bottom in this region, making it highly hazardous, though W_r is smaller in the foothills than in downstream reaches due to channel confinement. Within the alluvial valleys and transition to the plains, W_r increases and the net erosional signal begins to transition to net depositional, often abruptly. Avulsion and braiding dominate the channel response and W_r values peak here. Moving into the plains, net deposition occurs and the widening response diminishes as the coarse sediment load drops out of transport, flood flows spread out over wide valleys, and ω gradients diminish. Note that the downstream extent of elevated W_r values varies greatly among our study streams.

Our study area is a semi-arid environment that receives periodic extreme precipitation events due to the interaction of humid air currents with orographic lift from a mountain range (Gochis *et al.*, 2015). In addition to the hydroclimatology of the region, a sharp transition between steep, confined channels to less steep and unconfined channels from the foothills to the plains results in large gradients in transport capacity over short distances. During the 2013 flood, large quantities of sediment, sourced from debris flows and eroded channel margins were in transport within the steep, confined reaches of the foothills (Anderson *et al.*, 2015; Rathburn *et al.*, 2017). As indicated in our DoD analysis, the increased channel response (i.e. W_r) observed in areas of negative stream power gradient resulted from this sediment load via depositional processes. In terms of predicting the potential for and direction of channel response to floods, our findings may apply to other regions where longitudinal variations of channel confinement and slope interact with one another in similar manners. However, the magnitude of channel response is highly contextual resulting from the interaction of sediment and wood loads during flood events and boundary material resistance.

Reach-scale longitudinal patterns of ω, as well as ω gradient, can be evaluated for a channel network *a priori* for any frequency of flood using a DEM and a regional regression equation relating flood frequency and magnitude to remotely sensed variables, namely drainage area. Gartner *et al.* (2015) provide detailed methods for doing so. Channel confinement ratio can be evaluated manually using existing aerial imagery and DEMs. Data products and automated tools for delineating valley bottom width exist (Carlson, 2009; Roux *et al.*, 2015; Gilbert *et al.*, 2016), as well as other definitions of confinement ratio that may influence the relationship between channel confinement and flood response (Fryirs *et al.*, 2016). In sum, the data and tools required to evaluate the variables necessary to determine ω, ω_n and confinement ratio are readily available. These can be used to identify mild-sloped reaches with strongly negative stream power gradients (troughs and toes) as well as steep and confined reaches with elevated values of ω where major geomorphic response to floods can be expected. Quantitative predictions of, for example, W_n based on similar independent variables are not yet operational given the large variability in response and uncertainty associated with empirical models. However, upper bounds of response may be informative for floodplain management.
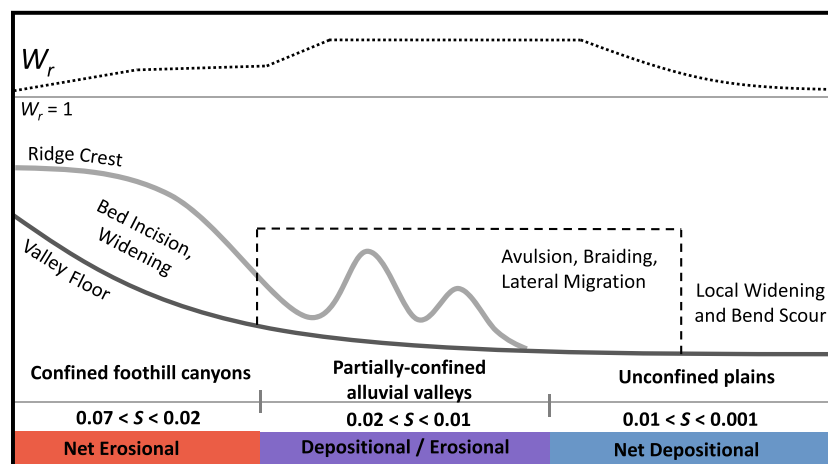

Figure 8. Conceptual figure showing downstream pattern of channel slope, confinement, and generalized width and sediment flux response within transition from foothills to plains after Bull (1988). Slope ranges will vary according to regional geology and unit peak discharge (m³ s⁻¹ km⁻²) (c.f., Flores et al., 2006; Hack, 1957). [Colour figure can be viewed at wileyonlinelibrary.com]

Conclusions

We measured channel width change (W_r) and net erosion and deposition (ΔV) at the reach (0.5 to 1 km) and segment scales (10 km) over 133 km of stream in three different basins impacted by the Colorado Front Range flood of 2013. These basins were all similar in that they transition from steep and confined headwaters reaches in the foothills to mild and unconfined mainstem reaches in the plains. This flood transported large sediment loads – sourced from debris flows and channel margins – from the foothills to the plains. We compared channel response metrics to estimates of flood peak unit stream power (ω), the ratio of downstream to upstream reach average ω (ω_r), and channel confinement by valley margins to evaluate how these variables influenced channel response. Based on our analysis and observations, we conclude that unit stream power gradient and channel confinement are significant predictors of reach-scale (0.5 to 1 km) and segment-scale (10 km) channel response to floods. However, the great variability in the relationships characterized herein highlights the existence and influence of other factors not incorporated into the present study. These include the inherent resistance of channel and valley margins to erosion as well as the role of vegetation in mediating channel response.

At the reach scale, we found that reductions in unit stream power in the downstream direction, or negative ω gradient (primary) and less channel confinement (secondary) are correlated with increases in the relative fluvial disturbance width. Less channel confinement (primary) and negative ω gradient (secondary) result in a net depositional response; whereas more channel confinement and positive ω gradient result in a net erosional response. However, ΔV was less sensitive to reach-scale ω gradient and followed segment-scale trends of net erosion in the foothills transitioning to net deposition in the plains. The largest channel response in terms of W_r and ΔV occurred in the transition from foothills (steep, confined) to plains (mild, unconfined) with a lag effect of elevated channel response up to 10 km downstream of the outlet of the canyons within the foothills. Spikes in W_r occurred at troughs and toes in the downstream longitudinal pattern of ω where the ω gradient is most strongly negative. There, relatively large widths of fluvial disturbance occurred at relatively low absolute values of ω. Away from these troughs and toes in ω, reach-scale ω_r values were less predictive of W_r.

Monotonic relationships between ω and channel response to floods do not apply within stream segments where substantial fluctuations in channel confinement and slope – and hence strongly negative ω gradients – exist. Relying on threshold values of ω, above which dramatic geomorphic response is expected, do not apply in these cases. Rather, consideration of the gradient of ω at the reach and segment scale is important for predicting channel response within these transitions. Future research should work to characterize the role of boundary resistance as well as sediment supply and transport capacity in mediating channel response to floods. Utilizing mechanistic sediment yield and transport models with field-based observational studies of extreme floods will aid in disentangling the complex responses that flood inevitably create.

References

Aggett GR, Wilson JP. 2009. Creating and coupling a high-resolution DTM with a 1-D hydraulic model in a GIS for scenario-based assessment of avulsion hazard in a gravel-bed river. *Geomorphology* **113**: 21–34.

Anderson RS, Riihimaki CA, Safran EB, MacGregor KR. 2006. Facing reality: late Cenozoic evolution of smooth peaks, glacially ornamented valleys, and deep river gorges of Colorado's Front Range. Special Paper 398: Tectonics, Climate, and Landscape Evolution. *Geological Society of America*: 397–418.

Anderson SW, Anderson SP, Anderson RS. 2015. Exhumation by debris flows in the 2013 Colorado Front Range storm. *Geology* **43**: 391–394.

ASFPM. 2016. Riverine erosion hazards. Madison, WI [online] Available from: https://www.floods.org/ace-images/ASFPMRiverine ErosionWhitePaperFeb2016.pdf

Bledsoe BP, Watson CC. 2001. Logistic analysis of channel pattern thresholds: meandering, braiding, and incising. *Geomorphology* **38**: 281–300.

Brierley GJ, Fryirs K. 2000. River Styles, a geomorphic approach to catchment characterization: implications for river rehabilitation in Bega catchment, New South Wales, Australia. *Environmental Management* **25**: 661–679.

Brierley GJ, Fryirs KA. 2005. *Geomorphology and River Management: Applications of the River Styles Framework.* Blackwell Publications: Oxford, UK.

Bull WB. 1988. *Floods; Degradation and Aggradation. Flood Geomorphology.* John Wiley and Sons: New York; 157–165.

Buraas EM, Renshaw CE, Magilligan FJ, Dade WB. 2014. Impact of reach geometry on stream channel sensitivity to extreme floods. *Earth Surface Processes and Landforms* **39**: 1–12. https://doi.org/10.1002/esp.3563.

Carlson EA. 2009. *Fluvial riparian classification for national forests in the western United States, Thesis (MS).* Colorado State University: Fort Collins, CO.

Cenderelli DA, Wohl EE. 2003. Flow hydraulics and geomorphic effects of glacial-lake outburst floods in the Mount Everest region, Nepal. *Earth Surface Processes and Landforms* **28**: 385–407.

Coe JA, Kean JW, Godt JW, Baum RL, Jones ES, Gochis DJ, Anderson GS. 2014. New insights into debris-flow hazards from an extraordinary event in the Colorado Front Range. *GSA Today* **24**(10): 4–10.

Costa JE, O'Connor JE. 1995. Geomorphically effective floods. In *Natural and Anthropogenic Influences in Fluvial Geomorphology,* Costa JE, Miller AJ, Potter KW, Wilcock PR (eds). American Geophysical Union: Washington, DC; 45–56.

Flores AN, Bledsoe BP, Cuhaciyan CO, Wohl EE. 2006. Channel-reach morphology dependence on energy, scale, and hydroclimatic processes with implications for prediction using geospatial data. *Water Resources Research* **42**: 1–15. https://doi.org/10.1029/2005Wr R004226.

Fryirs K, Brierley GJ. 2010. Antecedent controls on river character and behaviour in partly confined valley settings: Upper Hunter catchment, NSW, Australia. *Geomorphology* **117**: 106–120.

Fryirs KA, Wheaton JM, Brierley GJ. 2016. An approach for measuring confinement and assessing the influence of valley setting on river forms and processes. *Earth Surface Processes and Landforms* **41**: 701–710.

Gartner JD, Dade WB, Renshaw CE, Magilligan FJ, Buraas EM. 2015. Gradients in stream power influence lateral and downstream sediment flux in floods. *Geology* **43**: 983–986.

Gilbert JT, Macfarlane WW, Wheaton JM. 2016. The valley bottom extraction tool (V-BET): a GIS tool for delineating valley bottoms across entire drainage networks. *Computers and Geosciences* **97**: 1–14.

Giraudoux P. 2016. pgirmess: Data Analysis in Ecology [online] Available from: https://cran.r-project.org/package=pgirmess. Accessed April 10 2017.

Gochis D, Schumacher R, Friedrich K, Doesken N, Kelsch M, Sun J, Ikeda K, Lindsey D, Wood A, Dolan B, Matrosov S, Newman A, Mahoney K, Rutledge S, Johnson R, Kucera P, Kennedy P, Sempere-Torres D, Steiner M, Roberts R, Wilson J, Yu W, Chandrasekar V, Rasmussen R, Anderson A, Brow B. 2015. The Great Colorado Flood of September 2013. *Bulletin of the American Meteorological Society* **96**: 1461–1487.

Graf WL. 1983. Downstream changes in stream power in the Henry mountains, Utah. *Annals of the Association of American Geographers* **73**: 373–387.

Green GN. 1992. The Digital Geologic Map of Colorado in ARC/INFO Format. US Geologic Survey Open File Report 92-0507. http:/pubs.usgs.gov/of/1992/ofr-92-0507. Accessed 7 June 2016.

Hack JT. 1957. Studies of longitudinal stream profiles in Virginia and Maryland. USGS Professional Paper 294-B, 45–97. Washington, DC.

Hauer C, Habersack H. 2009. Morphodynamics of a 1000-year flood in the Kamp River, Austria, and impacts on floodplain morphology. *Earth Surface Processes and Landforms* **34**: 654–682.

Jarrett RD, Costa JE. 1988. Evaluation of the flood hydrology in the Colorado Front Range using precipitation, streamflow, and paleoflood data for the Big Thompson river basin. US Geological Survey, Water-Resources Investigations Report 87–4117.41.

Kean JW, McGuire LA, Rengers FK, Smith JB, Staley DM. 2016. Amplification of postwildfire peak flow by debris. *Geophysical Research Letters* **43**: 8545–8553.

Koenker R. 2016. quantreg: Quantile Regression [online] Available from: https://cran.r-project.org/package=quantreg. Accessed April 10, 2017.

Krapesch G, Hauer C, Habersack H. 2011. Scale orientated analysis of river width changes due to extreme flood hazards. *Natural Hazards and Earth System Sciences* **11**: 2137–2147.

Lea DM, Legleiter CJ. 2015. Mapping spatial patterns of stream power and channel change along a gravel-bed river in northern Yellowstone. *Geomorphology* **252**: 66–79.

Magilligan FJ. 1992. Thresholds and the spatial variability of flood power during extreme floods. *Geomorphology* **5**: 373–390.

McLeod AI. 2011. Kendall: Kendall rank correlation and Mann-Kendall trend test [online] Available from: http://cran.r-project.org/package=Kendall. Accessed April 10, 2017.

Miller AJ. 1990. Flood hydrology and geomorphic effectiveness in the central Appalachians. *Earth Surface Processes and Landforms* **15**: 119–134.

Miller AJ. 1995. Valley morphology and boundary conditions influencing spatial patterns of flood flow. In *Natural and Anthropogenic Influences in Fluvial Geomorphology*, Costa JE, Miller AJ, Potter KW, Wilcock PR (eds). Geophysical Monograph Series 89. American Geophysical Union: Washington, DC; 57–81.

Moody JA. 2016. Estimates of peak flood discharge for 21 sites in the Front Range in Colorado in response to extreme rainfall in September 2013. US Geological Survey, Scientific Investigations Report: 2016–5003. Boulder, CO.

Nanson GC, Croke JC. 1992. A genetic classification of floodplains. *Geomorphology* **4**: 459–486.

Nardi L, Rinaldi M. 2015. Spatio-temporal patterns of channel changes in response to a major flood event: the case of the Magra River (central-northern Italy). *Earth Surface Processes and Landforms* **40**: 326–339.

Parker C, Clifford NJ, Thorne CR. 2012. Automatic delineation of functional river reach boundaries for river research and applications. *River Research and Applications* **28**: 1708–1725.

Parker C, Thorne CR, Clifford NJ. 2015. Development of ST:REAM: a reach-based stream power balance approach for predicting alluvial river channel adjustment. *Earth Surface Processes and Landforms* **40**: 403–413.

Piégay H, Darby SE, Mosselman E, Surian N. 2005. A review of techniques available for delimiting the erodible river corridor: a sustainable approach to managing bank erosion. *River Research and Applications* **21**: 773–789.

R Core Team. 2016. *R: A Language and Environment for Statistical Computing*. R Foundation for Statistical Computing: Vienna, Austria.

Rathbun S, Bennett GL, Wohl EE, Briles C, McElroy B, Sutfin N. 2017. The fate of sediment, wood, and organic carbon eroded during an extreme flood, Colorado Front Range, USA. *Geology* **45**: 1–14. https://doi.org/10.1130/G38935.1.

Rinaldi M, Surian N, Comiti F, Bussettini M. 2013. A method for the assessment and analysis of the hydromorphological condition of Italian streams: The Morphological Quality Index (MQI). *Geomorphology* **180**: 96–108.

Rinaldi M, Amponsah W, Benvenuti M, Borga M, Comiti F, Lucía A, Lorenzo M, Nardi L, Righini M, Surian N. 2016. An integrated

approach for investigating geomorphic response to extreme events: methodological framework and application to the October 2011 flood in the Magra River catchment, Italy. *Earth Surface Processes and Landforms* **41**: 835–846.

Roux C, Alber A, Bertrand M, Vaudor L, Piégay H. 2015. 'FluvialCorridor': A new ArcGIS toolbox package for multiscale riverscape exploration. *Geomorphology* **242**: 29–37.

Siegel S, Castellan N. 1988. *Nonparametric Statistics for the Behavioral Sciences*, 2nd edn. New York: McGraw-Hill.

Surian N, Mao L, Giacomin M, Ziliani L. 2009. Morphological effects of different channel-forming discharges in a gravel-bed river. *Earth Surface Processes and Landforms* **34**: 1093–1107.

Surian N, Righini M, Lucía A, Nardi L, Amponsah W, Benvenuti M, Borga M, Cavalli M, Comiti F, Marchi L, Rinaldi M, Viero A. 2016. Channel response to extreme floods: Insights on controlling factors from six mountain rivers in northern Apennines, Italy. *Geomorphology* **272**: 78–91 http://doi.org/10.1016/j.geomorph.2016.02.002.

Tamminga AD, Eaton BC, Hugenholtz CH. 2015. UAS-based remote sensing of fluvial change following an extreme flood event. *Earth Surface Processes and Landforms* **40**: 1464–1476.

Thompson C, Croke J. 2013. Geomorphic effects, flood power, and channel competence of a catastrophic flood in confined and unconfined reaches of the upper Lockyer valley, southeast Queensland, Australia. *Geomorphology* **197**: 156–169.

Vocal-Ferencevic M, Ashmore P. 2012. Creating and evaluating digital elevation model-based stream-power map as a stream assessment tool. *River Research and Applications* **28**: 1394–1416.

Wheaton JM, Brasington J, Darby SE, Sear DA. 2010. Accounting for uncertainty in DEMs from repeat topographic surveys: improved sediment budgets. *Earth Surface Processes and Landforms* **35**: 136–156.

Wohl EE. 2010. A brief review of the process domain concept and its application to quantifying sediment dynamics in bedrock canyons. *Terra Nova* **22**: 411–416.

Wohl EE. 1992. Gradient irregularity in the herbert gorge of Northeastern Australia. *Earth Surface Processes and Landforms* **17**: 69–84.

Yochum SE, Sholtes JS, Scott JA, Bledsoe BP. 2017. Stream power and geomorphic change during the 2013 Colorado front range flood. *Geomorphology* **292**: 178–192.

Supporting Information

Additional supporting information may be found online in the Supporting Information section at the end of the article.

Table S1. LiDAR and DEM of difference error analysis.

Figure S2. (A) Kernel density functions of channel widths pre (solid) and post (dashed) flood within confined reaches (dark green) and partially and unconfined reaches (light green). Note positive skewness and width variability is much larger post flood and within less confined reaches. (B) Kernel density function for net unit volume change between confined (dark red) and partially and unconfined (light red) reaches.

Figure S3. Longitudinal relationship between confinement ratio (dark green line, right hand axis), unit stream power (dark grey polygons, left hand axis)), and W_{valley} / W_{post} (i.e., post-flood confinement ratio, turquoise line, right hand axis).

Figure S4. Boxplots of W_r for reaches in which the post-flood width of fluvial disturbance (W_{post}) equaled the valley width (left) (i.e., fluvial disturbance extended up to the valley margins and was potentially limited by these), and for reaches in which W_{post} was less than the valley width (right).

Figure S5. Boxplots of ω_r for reaches located at peaks in the downstream longitudinal pattern of ω, troughs and toes in ω, and other reaches in between these (unclassified) with a logarithmic scale on the y-axis. Negative ω gradients ($\omega_r < 1$) are primarily associated with troughs and toes, whereas peaks are associated with positive ω gradients ($\omega_r > 1$).

Figure S6. Boxplots of stream power gradient for categories of confinement (confined, C and unconfined, U) and landscape position (foothills, FH and plains, PL).

Figure S7. Boxplots of W_r and ΔV for reaches located at peaks in the longitudinal ω pattern (blue), troughs and toes (red), and for all other reaches not located at peaks or toughs (unclassified) discriminated by ω gradient: positive ($\omega_r > 1$) or negative ($\omega_r < 1$).

Figure S8. Boxplots of W_r and ΔV for reaches located at peaks in the longitudinal ω pattern (blue), troughs and toes (red), and for all other reaches not located at peaks or toughs (unclassified) discriminated by landscape position: foothills (FH) and plains (PL). Reach-scale ΔV is most strongly erosional for trough/toe reaches in the foothills and most strongly depositional for trough/toe reaches in the plains. This figure further affirms that landscape position most influences ΔV over reach-scale factors: the foothills are mostly degradational whereas the plains are mostly aggradational.

Table S2. Intercept and slope values for quantile regression of W_r as a function of $\log10(\omega_r)$. Confidence intervals at the 95% significance level are reported in parentheses below each value.